Investigation of the Electronic Structure of 2Fe−2S Model Complexes and the Rieske Protein Using Ligand K-Edge X-ray Absorption Spectroscopy

Kendra Rose,[†] Susan E. Shadle,[†] Thorsten Glaser,[†] Simon de Vries,[‡] Alexej Cherepanov,[‡] Gerard W. Canters,[§] Britt Hedman,*[,||] Keith O. Hodgson,*[,†,||] and Edward I. Solomon*[,†]

Contribution from the Department of Chemistry, Stanford University, Stanford, California 94305, Department of Microbiology and Enzymology, Technical University Delft, 2628 BC Delft, The Netherlands, Leiden Institute of Chemistry, Gorlaeus Laboratories, Leiden University, 2300 RA Leiden, The Netherlands, and Stanford Synchrotron Radiation Laboratory, SLAC, Stanford University, Stanford, California 94309

Received September 28, 1998. Revised Manuscript Received January 19, 1999

Abstract: X-ray absorption spectroscopy at the sulfur K-edge (∼2470 eV) has been applied to a series of 2Fe−2S model complexes to obtain insight into their electronic structures. Since these 2Fe−2S complexes contain both terminal thiolates and bridging sulfides, contributions to covalency from both sets of ligands can be evaluated. Importantly, the pre-edge feature of sulfide can be resolved from that of thiolate due to differences in effective nuclear charge. In our previous studies, the covalency of the metal−thiolate bond in $[Fe(SR)_4]^-$ was determined. In this study, sulfide covalency is quantified for the first time on the basis of an analysis of previous X-ray photoelectron and X-ray absorption spectroscopic studies of $[FeCl_4]^-$ which are then applied to the bis-μ_2-sulfide compound $KFeS_2$. With references for both sulfide and thiolate covalencies thus established for open d-shell systems, comparisons are made between thiolate and sulfide bonding. Sulfide−Fe covalency in the $[Fe_2S_2(SR)_4]^{2-}$ complexes is higher than thiolate−Fe covalency, indicating extensive charge donation of the bridging sulfides. Finally, this investigation of model complexes is extended to the oxidized and reduced 2Fe−2S cluster of the Rieske protein of *Paracoccus denitrificans* which has terminal thiolates on one Fe center, and histidines on the other Fe center. It is determined that thiolate covalency of the Fe(III) center is the same in both the oxidized and reduced Rieske clusters and similar to that of the $[Fe_2S_2(SR)_4]^{2-}$ model complexes. Further, in the fully oxidized Rieske cluster, the sulfide covalency of the ferric center containing terminal histidine ligation is ∼18% higher than the Fe(III) containing terminal thiolate ligation. This is consistent with the fact that the histidine ligands are poorer donors and supports the suggestion that the terminal histidine ligation makes a significant contribution to the higher reduction potential of the Rieske protein.

Introduction

Metalloproteins containing iron−sulfur active sites are present in all forms of life and are commonly involved in electron transfer.[1−5] The simplest of the Fe−S proteins are the rubredoxins which contain one iron center and often have molecular weights in the range of 6−7 kDa. The rubredoxin Fe site is coordinated by four thiolates from cysteine residues in a nearly T_d geometry.[6,7] In the 2Fe ferredoxins, the metal ions have terminal thiolate ligation as in the rubredoxins, but additionally have di-μ-bridging sulfides as shown in Figure 1a. The irons in the dimer are antiferromagnetically coupled through a superexchange pathway via the bridging sulfides.[8−10] The biologically relevant redox reaction of the 2Fe ferredoxins involves a one-electron couple between 2Fe(III) and an Fe(III)/Fe(II). The oxidized site has an $S = 0$ ground state, and the reduced state, which is a localized mixed valence site,[11] has an $S = 1/2$ ground state. The nature of the electronic structure of these iron−sulfur active sites and its relationship to electron-transfer reactivity is not yet fully understood. However, the highly covalent sulfur−metal interactions clearly play an important role in determining the reactivity of these sites. Investigating the ligand−metal bonding in the 2Fe−2S ferredoxin system is of critical importance in understanding this site and defining electronic structure contributions to reduction potentials and electron-transfer pathways.

Ligand K-edge X-ray absorption spectroscopy (XAS) provides a direct experimental probe of these ligand−metal bonding

* To whom correspondence should be addressed.
[†] Department of Chemistry, Stanford University.
[‡] Technical University Delft.
[§] Leiden University.
[||] Stanford Synchrotron Radiation Laboratory, SLAC, Stanford University.

(1) *Iron-Sulfur Proteins, Vol. I−III*; Lovenberg, W., Ed.; Academic Press: New York, 1973−1977.
(2) *Iron-Sulfur Proteins*; Spiro, T. G., Ed.; John Wiley & Sons: New York, 1982.
(3) *Iron-Sulfur Proteins*; Cammack, R., Ed.; Advances in Inorganic Chemistry; Academic Press: San Diego, CA, 1992.
(4) Beinert, H. *FASEB J.* **1990**, *4*, 2483−2491.
(5) Beinert, H.; Holm, R. H.; Münck, E. *Science* **1997**, *277*, 653−659.
(6) Day, M. W.; Hsu, B. T.; Joshua-Tor, L.; Park, J.-B.; Zhou, Z. H.; Adams, M. W. W.; Rees, D. C. *Protein Sci.* **1992**, *1*, 1494−1507.
(7) Dauter, Z.; Wilson, K. S.; Sieker, L. C.; Moulis, J.-M.; Meyer, J. *Proc. Natl. Acad. Sci. U.S.A.* **1996**, *93*, 8836−8840.
(8) Anderson, P. W. *Solid State Phys.* **1963**, *14*, 99−214.
(9) Hay, P. J.; Thibeault, J. C.; Hoffman, R. *J. Am. Chem. Soc.* **1975**, *97*, 4884−4899.
(10) de Loth, P.; Cassioux, P.; Daudey, J. P.; Malrieu, J. P. *J. Am. Chem. Soc.* **1981**, *103*, 4007−4016.
(11) Johnson, C. E. *J. Appl. Phys.* **1971**, *42*, 1325−1331.

10.1021/ja983455l CCC: $18.00
Published on Web 03/04/1999

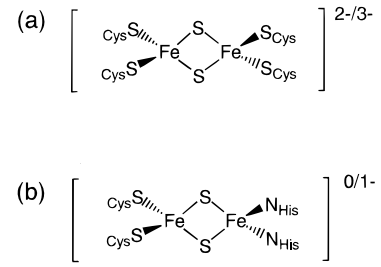

Figure 1. Schematic structures of the iron sulfur active sites in **(**a**)** the 2Fe ferredoxin site and **(**b**)** the Rieske protein.

interactions. The electric dipole-allowed transitions for K-edges are 1s → *n*p. The K-edge absorption of a ligand bound to a d^9 copper ion exhibits a well-defined pre-edge feature which is assigned as a ligand 1s → ψ^* transition, where ψ^* is the half-filled, highest-occupied molecular orbital (HOMO) in Cu(II).[12] Due to the localized nature of the ligand (L) 1s orbital, this transition can have absorption intensity only if the half-filled HOMO orbital contains a significant component of ligand 3p character as a result of covalency. The intensity of this L 1s → ψ^* transition is given by eq 1, where $\psi^* = (1 - \alpha'^2)^{1/2}$[Cu 3d]

$$I(\text{L 1s} \rightarrow \psi^*) = \alpha'^2\, I(\text{L 1s} \rightarrow \text{L 3p}) \qquad (1)$$

$- \alpha'$[L 3p] and α'^2 represents the amount of L 3p character in the HOMO. The observed pre-edge transition intensity is then the intensity of the pure dipole-allowed L 1s → L 3p transition weighted by α'^2. Thus, the pre-edge intensity provides a quantitative estimate of the ligand contribution to the HOMO due to bonding.

The pre-edge feature in d^n metal centers other than Cu(II) also corresponds to a transition (or several transitions) from a ligand 1s orbital to unoccupied or partially occupied antibonding orbitals with both metal d and ligand p character. However, in systems with more than one d-manifold electron or hole, transitions to more than one partially occupied metal d-derived orbital are possible and multiplet effects in the d^{n+1} final state can affect the observed intensity. Methodology has been developed to analyze these effects for the Cl K-edge pre-edge intensity in a series of tetrahedral metal tetrachlorides, $[MCl_4]^{2-}$, where M = Cu(II), Ni(II), Co(II), and Fe(II).[13a] The correlation between S pre-edge intensity and covalency has also been developed for an analogous $[M(SR)_4]^{2-}$ series, where M = Ni-(II), Co(II), Fe(II), and Mn(II).[14] It is important to note that in these tetrathiolate complexes the anisotropy of the thiolate p orbitals in bonding to the metal has to be taken into account. On the basis of the $[MCl_4]^{2-}$ and $[M(SR)_4]^{2-}$ studies, expressions have been derived for metal centers, which allows the ligand HOMO covalency to be quantitatively related to ligand pre-edge intensity.[13a,14] This expression for tetrahedral ferric complexes is given in eq 2.[13b] D_0 is the total experimental

$$D_0(\text{Fe(III)}) = (c_1^{\,2} + c_2^{\,2} + (2/3)c_3^{\,2})\langle \text{s}|\mathbf{r}|\text{p}\rangle^2 \qquad (2)$$

intensity, c_1^2 and c_2^2 are coefficients which reflect the ligand 3p σ and π covalency, respectively, in the t_2 set of orbitals, c_3^2 is the coefficient which reflects π covalency in the e set of orbitals, and $\langle \text{s}|\mathbf{r}|\text{p}\rangle^2$ is the intensity of a pure ligand 1s → 3p transition. Thus, ligand K-edge XAS can provide a direct experimental probe of the ligand character in the redox active orbitals in Fe−S systems.

Recently, ligand K-edge XAS has been applied to investigate the monomeric iron tetrathiolate systems.[15] A study of ferrous and ferric model complexes and a series of rubredoxins was performed. In that study, it was established that the ferric model complex had a S K-edge pre-edge feature that was similar in shape and energy to that of the proteins. It was determined, however, that the covalencies of the proteins were lower than that of the model complex. This is consistent with the fact that H-bonding reduces the ability of the sulfur to donate electron density to the metal. It was further established, on the basis of the S K-edge spectrum of a ferrous monomer in the rubredoxin study,[15] and the previous metal tetrathiolate study,[14] that the pre-edge feature of the ferrous complex is shifted to higher energy and overlaps the S edge due to the lower effective nuclear charge on the ferrous site. These results are important for the extension to higher nuclearity iron−sulfur systems.

In this work, sulfur K-edge XAS studies have been conducted for a series of binuclear iron−sulfur model complexes whose structural properties as well as synthetic references are given in Table 1. Analysis of the S K-edges of a series of binuclear iron−sulfur sites defines the covalency of the thiolate S−Fe-(III) bond and also the bridging sulfide−Fe(III) bond and provides a reference for binuclear ferric sites in proteins. The S K-edge XAS of $[Fe_2Se_2(SPh)_4]^{2-}$ and $[Fe_2S_2Cl_4]^{2-}$, which contain contributions from only thiolate or bridging sulfide, respectively, have been compared to assign the pre-edge transitions of the $[Fe_2S_2(SR)_4]^{2-}$ spectra. In addition, although iron−thiolate covalency has been previously investigated and determined, the covalency of an iron-bridging sulfide bond has not been established. In this study, a reference is established for quantifying iron−sulfide covalency using photoelectron spectroscopy and XAS data. The total covalencies of the dimeric iron−sulfur models are then determined, individual contributions of the ligands to iron−sulfur covalency are investigated, and experimentally determined covalencies are correlated with redox properties. A comparison is made between the 2Fe−2S model complexes and the oxidized and reduced Rieske protein.

The Rieske cluster of *Paracoccus denitrificans*, which is depicted in Figure 1b, is part of the membrane-bound cytochrome bc_1 complex, which participates in aerobic mitochondrial or bacterial respiratory chains and in the photoredox chains in purple bacteria.[17] The function of the Rieske cluster is to catalyze the one-electron oxidation of hydroquinone to the semiquinone followed by one-electron transfer to a *c*-type cytochrome (c_1 or *f*). The Rieske cluster is similar to the ferredoxin center in that it is a binuclear site containing di-μ-bridging sulfides between the two iron atoms.[18] However, while one of the iron ions of the Rieske cluster has terminal thiolate ligation consistent with the 2Fe ferredoxin, the other iron site contains nitrogen ligation from histidines (Figure 1b). The Rieske cluster has a high reduction potential of 140−290 mV,[19] and the reduction occurs

(12) Hedman, B.; Hodgson, K. O.; Solomon, E. I. *J. Am. Chem. Soc.* **1990**, *112*, 1643−1645.

(13) (a) Shadle, S. E.; Hedman, B.; Hodgson, K. O.; Solomon, E. I. *J. Am. Chem. Soc.* **1995**, *117*, 2259−2272. (b) Note that the R^2 term in Table 6 of ref 13a is not appropriate for a core to valence CT transition: Neese, F.; Solomon, E. I. Unpublished results.

(14) Rose Williams, K.; Hedman, B.; Hodgson, K. O.; Solomon, E. I. *Inorg. Chim. Acta* **1997**, *263*, 315−321.

(15) Rose, K.; Shadle, S. E.; Eidsness, M. K.; Kurtz, D. K., Jr.; Scott, R. A.; Hedman, B.; Hodgson, K. O.; Solomon, E. I. *J. Am. Chem. Soc.* **1998**, *120*, 10743−10747.

(16) Holm, R. H.; Berg, J. M. In *Iron-Sulfur Proteins*; Spiro, T. G., Ed.; John Wiley & Sons: New York, 1982; pp 1−66.

(17) de Vries, S.; Cherepanov, A.; Berg, A.; Canters, G. W. *Inorg. Chim. Acta* **1998**, *275*−*276*, 493−499.

(18) Iwata, S.; Maynovits, M.; Link, T. A.; Michel, H. *Structure* **1996**, *4*, 567−579.

(19) Link, T. A.; Hagen, W. R.; Pierik, A. J.; Assmann, C.; Von Jagow, G. *Eur. J. Biochem.* **1992**, *208*, 685−691.

Table 1. Summary of 2Fe−2S Model Complex Structures[a]

sample	iron coordination	av Fe−S* (Å)	av Fe−SR (Å)	X−Fe−X (deg)	Fe−Fe (Å)	synth ref	cryst struct ref
$[Et_4N]_2[Fe_2S_2(S\text{-}o\text{-}xyl)_2]$	$FeS^*_2(SR)_2$	2.208	2.304	104.7−112.3	2.698	22	51
$[Me_3NCH_2Ph]_2[Fe_2S_2(SEt)_4]$	$FeS^*_2(SR)_2$	ND				21	
$[Et_4N]_2[Fe_2S_2(SPh)_4]$	$FeS^*_2(SR)_2$	2.198	2.301	111.8−119.8	2.691	22	52
$[Et_4N]_2[Fe_2S_2Cl_4]$	$FeS^*_2Cl_2$	2.200	2.251[b]	105.4−112.7	2.716	23	53
$[Et_4N]_2[Fe_2Se_2(SPh)_4]$	$FeSe^*_2(SR)_2$	2.328[c]	2.306	106.2−113.1	2.795	22	49
$CsFe(III)S_2$	FeS^*_4	2.23		104.6−113.5	2.715	24	24

[a] ND = crystal structure not determined; An asterisk indicates a bridging sulfide/selenide. [b] Fe−Cl distance. [c] Fe−Se distance.

at the iron atom that contains the terminal histidine ligation.[20] Therefore, due to similarities to the ferredoxins, the ability to selectively reduce one of the iron atoms in the protein, and the high reduction potential, these model studies have been extended to the Rieske protein. The covalencies of both the terminal thiolates and bridging sulfides to the Fe(III) center in the protein and differences in the oxidized sites due to ligation differences are investigated.

Experimental Section

Sample Preparation. The model complexes $[Me_3NCH_2Ph]_2[Fe_2S_2(SEt)_4]$,[21] $[Et_4N]_2[Fe_2S_2(SPh)_4]$,[22] $[Et_4N]_2[Fe_2S_2(S\text{-}o\text{-}xyl)_2]$,[22] $[Et_4N]_2[Fe_2Se_2(SPh)_4]$,[22] $[Et_4N]_2[Fe_2S_2Cl_4]$,[23] and $CsFeS_2$,[24] as well as the water-soluble fragment of the Rieske protein from *Paracoccus denitrificans*,[17] were prepared according to published procedures.

For the XAS experiments, the solid samples of model complexes were ground into a fine powder which was dispersed as thinly as possible on Mylar tape to minimize the possibility of self-absorption. The procedure has been verified to minimize self-absorption effects in the data by systematically testing progressively thinner samples until the observed intensity no longer varies with the thickness of the sample. The Mylar tape contained an acrylic adhesive which was determined to have a level of sulfur and chlorine contaminants below that which is detectable under the conditions of the X-ray absorption measurements. The powder on tape was mounted across the window of an aluminum plate. The samples were prepared in dry, anaerobic atmospheres. A 6.35 μm polypropylene film window protected the solid samples from exposure to air during transfer from a nitrogen-filled glovebox to the experimental sample chamber.

The protein samples were preequilibrated in a water-saturated He atmosphere for ∼0.5−1 h to minimize bubble formation in the sample cell. Protein solutions were loaded via a syringe into a Pt-coated Al block sample holder sealed in front by a 6.35 μm thick polypropylene window. The protein concentrations were 0.8−1.0 mM in 20 mM potassium phosphate buffer. After several scans of the initially reduced Rieske protein were obtained, the sample was oxidized with approximately 2−3 equiv of a 100 mM solution of $K_3[Fe(CN)_6]$ prepared in deionized water.

X-ray Absorption Spectroscopy Measurements. XAS data were measured at the Stanford Synchrotron Radiation Laboratory using the 54-pole wiggler beamline 6-2 in a high magnetic field mode of 10 kG with a Ni-coated harmonic rejection mirror and a fully tuned Si(111) double crystal monochromator, under ring conditions of 3.0 GeV and 50−100 mA. The entire path of the beam was in a He atmosphere. Details of the optimization of this setup for low-energy studies have been described in an earlier publication.[25]

All S K-edge XAS measurements were made at room temperature for the solid samples, and ∼4 °C for the proteins. The data were measured as fluorescence excitation spectra utilizing an ionization chamber as a fluorescence detector.[26,27] To check for reproducibility, at least 2−3 scans were measured for each solid sample, while multiple scans were measured of the proteins to obtain a good signal-to-noise level in the data and to monitor photoreduction of the samples. The final averages for the proteins were based on five and twelve scans for the oxidized and reduced Rieske protein, respectively. The energy was calibrated from S K-edge spectra of $Na_2S_2O_3\cdot 5H_2O$, which were collected at intervals between the samples. The maximum of the first pre-edge feature in the spectrum was assigned to 2472.02 eV. Scans ranged from 2420 to 2740 eV and from 2440 to 2525 eV for models and proteins, respectively, with a step size of 0.08 eV in the edge region. The spectrometer energy resolution was ∼0.5 eV.[25] Calculating and comparing first and second derivatives for model compounds measured repeatedly during different experimental sessions results in a reproducibility in edge position of ∼0.1 eV.

Cl K-edge measurements were made in an experimental manner analogous to that of the S K-edge measurements. The energy was calibrated from the Cl K-edge spectra of $Cs_2[CuCl_4]$, run at intervals between the samples. The maximum of the first edge-region feature in the spectrum was assigned to 2820.20 eV. Scans ranged from 2740 to 3100 eV, with a step size of 0.08 eV in the edge region for the samples.

Data Reduction. Data were averaged, and a smooth background was removed from all spectra by fitting a polynomial to the pre-edge region and subtracting this polynomial from the entire spectrum. Normalization of the data was accomplished by fitting a flat polynomial or straight line to the post-edge region and normalizing the edge jump to 1.0 at 2490 and 2820 eV for the S K-edge and Cl K-edge data, respectively.

Fitting Procedures. The intensities of pre-edge features of the ferric model complexes and the oxidized and reduced protein were quantified by fits to the data. The fitting program EDG_FIT, which utilizes the double precision version of the public domain MINPAK fitting library,[29] was used. EDG_FIT was written by Dr. Graham N. George of the Stanford Synchrotron Radiation Laboratory. Pre-edge features were modeled by pseudo-Voigt line shapes (simple sums of Lorentzian and Gaussian functions). This line shape is appropriate as the experimental features are expected to be a convolution of the Lorentzian transition envelope[30] and the Gaussian line shape imposed by the spectrometer optics.[27,31,32] A fixed 1:1 ratio of Lorentzian to Gaussian contribution for the pre-edge feature successfully reproduced these spectral features. The rising edge functions were also pseudo-Voigt line shapes, for which the Gaussian−Lorentzian mixture was allowed to vary to give the best empirical fit. Good fits which were used in the calculation of pre-edge peak intensity were those which were optimized to reproduce both the data and the second derivative of the data using a minimum number of

(20) Fee, J. A.; Findling, K. L.; Yoshida, T.; Hille, R.; Tarr, G. E.; Hearshen, D.; Dunham, W. R.; Day, E. P.; Kent, T. A.; Münck, E. *J. Biol. Chem.* **1984**, *259*, 124−133.
(21) Hagen, K. S.; Watson, A. D.; Holm, R. H. *J. Am. Chem. Soc.* **1983**, *105*, 3905−3913.
(22) Reynolds, J. G.; Holm, R. H. *Inorg. Chem.* **1980**, *19*, 3257−3260.
(23) Do, Y.; Simhon, E. D.; Holm, R. H. *Inorg. Chem.* **1983**, *22*, 3809−3812.
(24) Nishi, M.; Ito, Y.; Ito, A. *J. Phys. Soc. Jpn.* **1983**, *52*, 3602−3610.
(25) Hedman, B.; Frank, P.; Gheller, S. F.; Roe, A. L.; Newton, W. E.; Hodgson, K. O. *J. Am. Chem. Soc.* **1988**, *110*, 3798−3805.
(26) Stern, E. A.; Heald, S. M. *Rev. Sci. Instrum.* **1979**, *50*, 1579−1582.
(27) Lytle, F. W.; Greegor, R. B.; Sandstrom, D. R.; Marques, E. C.; Wong, J.; Spiro, C. L.; Huffman, G. P.; Huggins, F. E. *Nucl. Instrum. Methods* **1984**, *226*, 542−548.
(28) Shadle, S. E.; Penner-Hahn, J. E.; Schugar, H. J.; Hedman, B.; Hodgson, K. O.; Solomon, E. I. *J. Am. Chem. Soc.* **1993**, *115*, 767−776.
(29) Garbow, B. S.; Hillstrom, K. E.; More, J. J., Argonne National Laboratory.
(30) Agarwal, B. K. *X-ray Spectroscopy*; Springer-Verlag: Berlin, 1979.
(31) Lytle, F. W. In *Applications of Synchrotron Radiation*; Winick, H., Xian, D., Ye, M. H., Huang, T., Eds.; Gordon & Breach: New York, 1989; p 135.
(32) Tyson, T. A.; Roe, A. L.; Frank, P.; Hodgson, K. O.; Hedman, B. *Phys. Rev. B* **1989**, *39A*, 6305−6315.

peaks. It was determined, on the basis of the second derivative, that the sulfide pre-edge transition contained at least two peaks, and the thiolate at least one peak. Therefore, on the basis of the half-widths of 0.5−0.6 eV,[28] the transitions were fit with two and one peak, respectively. Single peak fits with a larger half-width were also performed. It should also be noted that a five-peak theoretical fit of the pre-edge of $[Et_4N]_2[Fe_2Se_2(SPh)_4]$ (vide infra) and a four-peak theoretical fit of $[Et_4N]_2[Fe_2S_2Cl_4]$ were performed to evaluate the effects of d-orbital splitting, but were not used in the final calculations of covalency for these complexes. Fits were performed over several energy ranges: from one which included the tail of the rising edge, to one which included the white line maximum of the edge. The intensity of a pre-edge feature (where peak intensity is given by peak area, calculated as the height × full width at half-maximum) is the sum of the intensity of all the pseudo-Voigts which successfully fit the feature for a given fit. The final reported intensity values for both the model complexes and the proteins were calculated by averaging all of the good pre-edge fits.

Error Sources and Analysis. There are several possible sources of systematic error in the analysis of these spectra. Normalization procedures can introduce a 1−3% difference in pre-edge peak heights, as determined by varying the parameters used to normalize a set of Cl K-edge spectra such that the final fits met requirements of consistency. The error for the intensity of a pure 1s → 3p transition was calculated for both sulfide and thiolate on the basis of $CsFeS_2$ and plastocyanin. For each sample, the standard deviation of the average of the pre-edge areas for the acceptable series of fits described in the previous section was calculated to quantify the uncertainty of the fit. The normalization error of ∼3% and the error resulting from the fitting procedure were combined (i.e., the square root of the sum of their squares) and propagated along with the error for the integral of the pure 1s → 3p transition. The uncertainty in pre-edge energies is limited by the reproducibility of the edge spectra (±0.1 eV).

Results

The S K-edge XAS spectra of the ferric model complexes $[Me_3NCH_2Ph]_2[Fe_2S_2(SEt)_4]$, $[Et_4N]_2[Fe_2S_2(S_2\text{-}o\text{-xyl})_2]$, and $[Et_4N]_2[Fe_2S_2(SPh)_4]$ are shown in Figure 2a. The pre-edge features of all three complexes occur between 2468 and ∼2472 eV. The edge feature which occurs between ∼2472 and 2474 eV shifts on the basis of the nature of the terminal thiolate ligation. The energies of these features are given in Table 2. These energies are based on fits to the second derivative of the data. A representative fit along with the second derivative is shown in Figure 2b,c. Since the edge feature of $[Et_4N]_2[Fe_2S_2(SPh)_4]$ (dotted line) has the highest energy and the most well-resolved pre-edge transitions, the S K-edge spectrum of this complex will be the focus of the study of the model complexes.

The S K-edge XAS spectra of $[Et_4N]_2[Fe_2Se_2(SPh)_4]$, $[Et_4N]_2[Fe_2S_2Cl_4]$, and $[Et_4N]_2[Fe_2S_2(SPh)_4]$ are shown in Figure 3a. The $[Et_4N]_2[Fe_2Se_2(SPh)_4]$ spectrum contains contributions from terminal thiolate ligation only, while that of $[Et_4N]_2[Fe_2S_2Cl_4]$ contains only bridging inorganic sulfide contributions. Therefore, energies and intensities of the pre-edge features of a sulfide and a thiolate in an iron−sulfur dimer can be determined, and the sum of the S K-edge spectra of these two complexes assumed to represent the total sulfur contributions from a $[Fe_2S_2(SR)_4]^{2-}$ complex. As seen from Figure 3b, using $[Et_4N]_2[Fe_2Se_2(SPh)_4]$ as a reference for terminal thiolate−Fe bonding and $[Et_4N]_2[Fe_2S_2Cl_4]$ for bridging sulfide−Fe bonding, the appropriately normalized sum of these data is a good representation for the S K-edge spectrum of $[Et_4N]_2[Fe_2S_2(SPh)_4]$. The peak at ∼2469.6 eV can be assigned as the sulfide 1s → Fe 3d and the peak at 2470.8 eV as the thiolate 1s → Fe 3d transition. The magnitude in energy separation, due to the difference in effective nuclear charge of the sulfide versus the thiolates, enables the pre-edge intensities to be resolved. The resulting covalency values obtained for sulfide and thiolate per iron for the model complexes shown in Figures 2 and 3 are given in Table 3, and renormalization of the data and calculations of the covalency are discussed in the Analysis section.

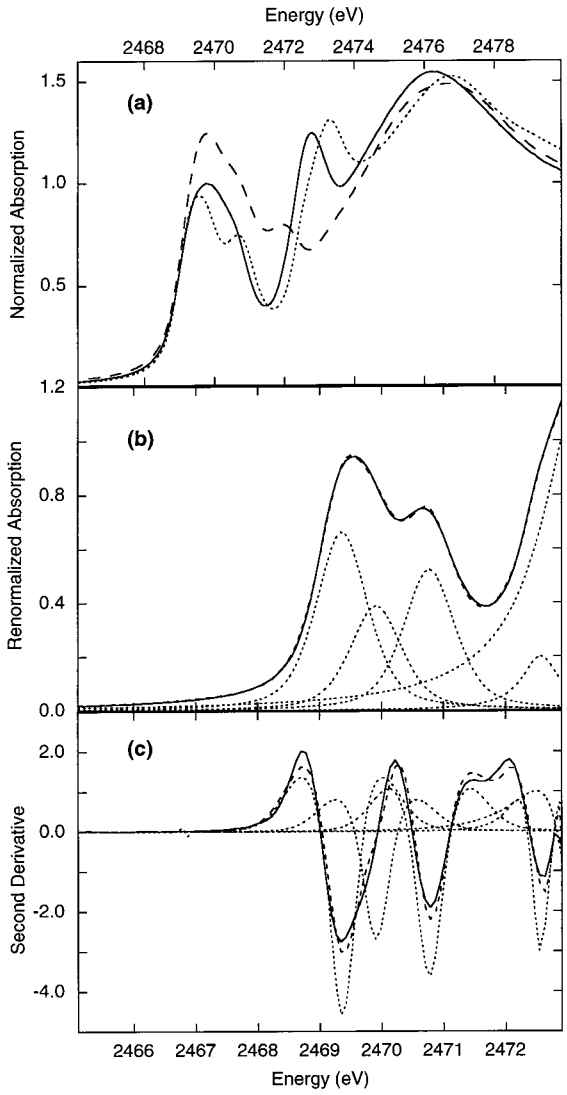

Figure 2. **(a)** S K-edge spectra of the fully oxidized 2Fe−2S model complexes: $[Me_3NCH_2Ph]_2[Fe_2S_2(SEt)_4]$ (—), $[Et_4N]_2[Fe_2S_2(S_2\text{-}o\text{-xyl})_2]$ (---), and $[Et_4N]_2[Fe_2S_2(SPh)_4]$ (•••). **(b)** Representative fit to the pre-edge region of the S K-edge spectrum of $[Et_4N]_2[Fe_2S_2(SPh)_4]$. **(c)** Second derivative of both the data (—) and the fit (---) to the data. Note that the energy scale of (a) is different from those of (b) and (c).

It has previously been established that the blue copper protein plastocyanin (Pc) has a S−Cys covalency of 38%,[28] and this has been used as a reference for quantifying thiolate covalency when a thiolate is bound to open-shell metal ions. There has been no reference established to correlate pre-edge intensity to covalency in an open-shell metal−sulfide bond. Therefore, the $CsFeS_2$ infinite chain complex, which contains bis-μ_2-sulfide bridges, has also been investigated in this study as a reference for bridging sulfide−Fe covalency. The S K-edge spectrum of $CsFeS_2$ is presented in Figure 4 along with that of $[Et_4N]_2[Fe_2S_2Cl_4]$ (from Figure 3a) for comparison. Since the features of these two spectra are similar, $CsFeS_2$ is appropriate for use as a reference compound.

To determine the total covalency in the dimers (vide infra), Cl K-edge data were also obtained for $[Et_4N]_2[Fe_2S_2Cl_4]$, shown in Figure 5. The spectrum of monomeric $[Et_4N][FeCl_4]$ is included as a reference.[13a] The edge energy decreases and the

Table 2. Sulfide and Thiolate Pre-edge and Thiolate S K-Edge Peak Energies[a]

compound	av sulfide energy[b] pre-edge peak 1	av sulfide energy[b] pre-edge peak 2	thiolate pre-edge peak energy[b]	thiolate peak edge energy[b]
$[Fe(S_2\text{-}o\text{-}xyl)_4]^-$			2470.4	2472.2
$[Fe_2S_2(SPh)_4]^{2-}$	2469.4	2469.9	2470.8	2472.7
$[Fe_2S_2(S_2\text{-}o\text{-}xyl)_2]^{2-}$	2469.5	2470.0	2470.7	2471.9
$[Fe_2S_2(SEt)_4]^{2-}$	2469.4	2470.0	2470.6	2472.7
$[Fe_2Se_2(SPh)_4]^{2-}$			2470.7	2472.5
$[Fe_2S_2Cl_4]^{2-}$	2469.3	2469.9		
$CsFeS_2$	2469.7	2470.3		
Rieske, oxidized	2469.3	2469.8	2470.8	2472.7
Rieske, reduced	2469.3	2469.9	2470.8	2472.6

[a] Energies are reported as average energies based on fits of the data. These fits are performed to reproduce the features of the second derivative of the data. Therefore, although theoretically there are five peaks representing the sulfide transition and four peaks representing the thiolate transition, the fits are based on two peaks in the sulfide (representing e and t_2 splitting) and one peak in the thiolate. [b] Units are electronvolts.

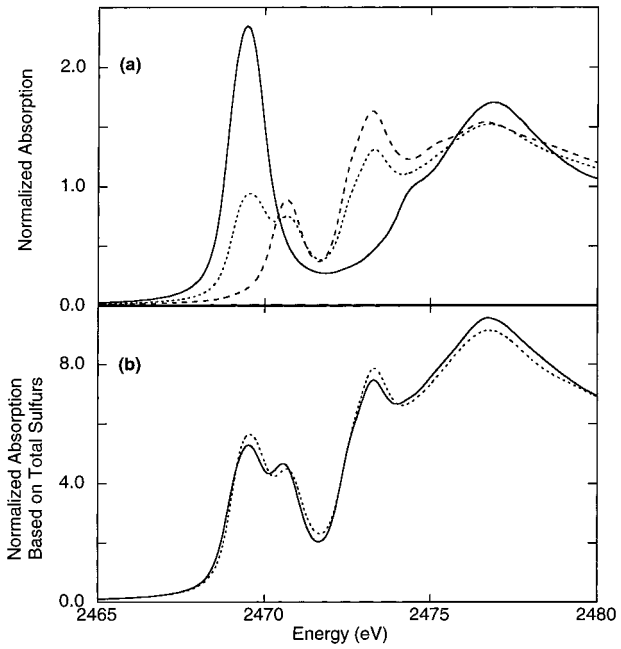

Figure 3. **(a)** Normalized S K-edge spectra of $[Et_4N]_2[Fe_2S_2Cl_4]$ (—), $[Et_4N]_2[Fe_2Se_2(SPh)_4]$ (---), and $[Et_4N]_2[Fe_2S_2(SPh)_4]$ (···). Note that the thiolate and sulfide pre-edge peaks are distinguishable in $[Et_4N]_2[Fe_2S_2(SPh)_4]$. **(b)** Addition of S K-edge spectra of $[Et_4N]_2[Fe_2S_2Cl_4]$ and $[Et_4N]_2[Fe_2Se_2(SPh)_4]$ (—) and comparison to that of $[Et_4N]_2[Fe_2S_2(SPh)_4]$ (---). The solid line was obtained by adding 2/1 of the S K-edge spectrum of $[Et_4N]_2[Fe_2S_2Cl_4]$ and 4/1 of the S K-edge spectrum of $[Et_4N]_2[Fe_2Se_2(SPh)_4]$.

pre-edge energy increases from monomer to dimer. In addition, the intensity of this pre-edge feature decreases from the monomer to the dimer, indicative of lower covalency in the dimeric complex. The total chloride−Fe covalency was determined to be 54% in the dimer, which corresponds to 27% chloride−Fe covalency per iron center.

The S K-edge data of both the oxidized (dashed line) and the reduced (solid line) Rieske protein are shown in Figure 6. The pre-edges of the reduced protein and the $[Et_4N]_2[Fe_2S_2(SPh)_4]$ model (dotted spectrum in Figure 3a) are similar in that they are both split with approximately the same energy difference. Previous studies showed that an Fe(II) center does not display a pre-edge feature that was energy resolved from the edge.[14,15] Therefore, the S K-edge spectrum of the reduced

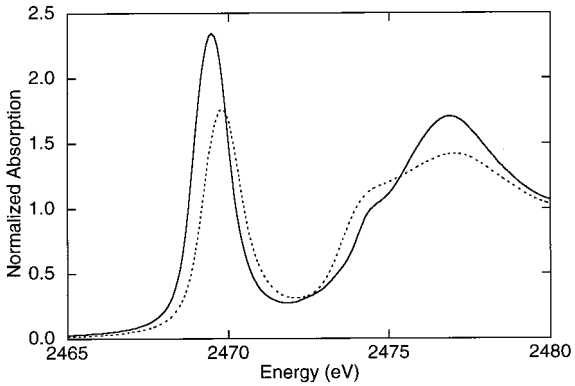

Figure 4. S K-edge spectra of $[Et_4N]_2[Fe_2S_2Cl_4]$ (—) and the infinite chain complex $CsFeS_2$ (···).

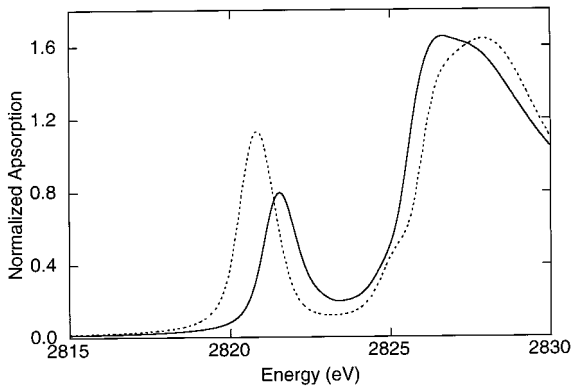

Figure 5. Cl K-edge spectra of $[Et_4N]_2[Fe_2S_2Cl_4]$ (—) and $[Et_4N][FeCl_4]$ (···).

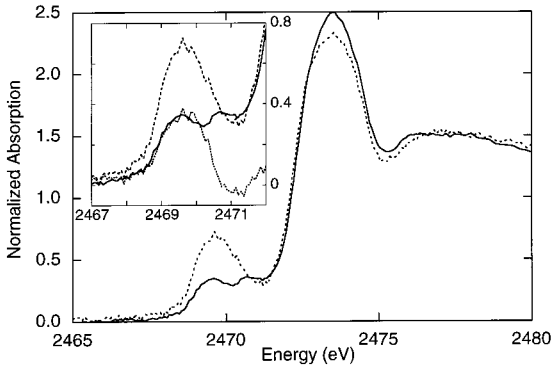

Figure 6. Normalized S K-edge spectra of the oxidized (Fe(III)/Fe(III)) (---) and the reduced (Fe(III)/Fe(II)) (—) Rieske protein. The inset shows an expanded pre-edge region and the difference spectrum of the oxidized and reduced clusters (···).

Rieske protein is a representation of thiolate and sulfide bonding to the oxidized iron site. Subtraction of the S K-edge spectrum of the reduced Rieske protein from the spectrum of the oxidized Rieske protein (inset of Figure 6) provides a means of quantifying the covalency of the individual sites in the oxidized protein. The values for the thiolate−Fe and sulfide−Fe covalency in both the reduced and oxidized protein are given in Table 3.

Analysis

Thiolate−Fe Bonding. As mentioned, the metal−ligand covalency is directly related to the intensity of the ligand pre-edge feature. To determine the metal−ligand covalency in the Fe−thiolate bond, the intensity of the pre-edge feature of the well-understood blue copper protein, plastocyanin, was used as

Table 3. Intensities and Covalencies[a] of S K-Edge Pre-edge Data

compound	sulfide intensity	renorm factor	renorm sulfide intensity	covalency of one sulfide per Fe (%)	thiolate intensity	renorm factor	renorm thiolate intensity	covalency of one thiolate per Fe (%)
$[Fe(S_2\text{-}o\text{-}xyl)_4]^-$					1.15	1	1.15	43 ± 2
$[Fe_2S_2(SPh)_4]^{2-}$	1.05	3	3.15	72 ± 5	0.53	1.5	0.80	30 ± 3
$[Fe_2S_2(S_2\text{-}o\text{-}xyl)_2]^{2-}$	1.46	3	4.38	100 ± 7	0.58	1.5	0.87	33 ± 2
$[Fe_2S_2(SEt)_4]^{2-}$	1.13	3	3.39	78 ± 7	0.45	1.5	0.67	25 ± 3
$[Fe_2Se_2(SPh)_4]^{2-}$					0.84	1	0.84	31 ± 2
$[Fe_2S_2Cl_4]^{2-}$	2.84	1	2.84	65 ± 5	0.94[b]	1[b]	0.94[b]	13 ± 2[b]
$CsFeS_2$	2.42	1	2.42	52 ± 5				
Rieske, oxidized	0.77	4	3.09	71 ± 7	0.23	4	0.91	34 ± 4
Rieske, reduced	0.36	4	1.45	67 ± 6	0.22	4	0.87	32 ± 3

[a] The covalency values are calculated on the basis of the intensities given and the use of eq 2. [b] Values for chloride.

the reference. For plastocyanin, this pre-edge feature has an intensity of 1.02 units, which corresponds to a covalency of 38% S−Cys in the Cu−S bond.[28] This intensity of the pre-edge feature is normalized to one sulfur; therefore, to determine the total covalency of the iron−thiolate bonds, the intensity of the pre-edge feature of the sample of interest needs to be multiplied by a factor representing the number of iron−thiolate bonds. Also, effective nuclear charge differences between the Cu(II) and Fe(III) complexes need to be taken into account when the total covalency is calculated (eq 2); however, it has been previously determined that this difference has a negligible effect.[13a]

For the 2Fe−2S complexes containing terminal thiolate ligation, the final covalency values were obtained after the data were renormalized to account for additional sulfurs present. Renormalization is performed to quantify the intensity of a pre-edge per one sulfide or one thiolate ligand, as all sulfurs in the complex contribute to the edge intensity, but only those bound to the iron site contribute to pre-edge intensity. Additionally, since the sulfide and the thiolate contributions to the pre-edge are resolved, renormalization needs to be performed for each type of sulfur. For example, for $[Et_4N]_2[Fe_2S_2(SPh)_4]$, the area of the peak representing the thiolate pre-edge intensity was multiplied by 6/4 since there are 6 total sulfurs present with 4 being thiolates contributing to the pre-edge intensity at ~2470.8 eV. For the bridging sulfides in the same complex, the renormalization factor was 6/2 since there are 6 total sulfurs, but only 2 of those sulfurs contribute to that specific pre-edge peak intensity. The S−K pre-edge intensity of $[Et_4N]_2[Fe_2Se_2(SPh)_4]$ was renormalized by a factor of 1 since all of the sulfurs present in the sample contribute to both edge and pre-edge intensities. After the thiolate pre-edge intensities were renormalized, the covalencies in Table 3 were calculated using eq 2 and the pre-edge intensity of the complexes. Note that the Rieske protein studied contains eight different sulfur atoms, two from methionine residues, four from cysteine residues, and two bridging sulfides. Only the two cysteines bound to the iron and the two bridging sulfides contribute to the pre-edge intensity, but all eight sulfurs contribute to the edge. Therefore, the pre-edge intensities for the thiolates and sulfides have been renormalized by a factor of 8/2.

Sulfide−Fe Bonding. To evaluate the sulfide covalency in the iron−sulfur clusters, a standard relating sulfide pre-edge peak intensity to covalency in open d-shell systems was needed, in analogy to the standard for thiolate covalency, as described above. In this paper this is established from the analysis of published XPS data on $KFeS_2$ using $Na[FeCl_4]$ as a reference.[33] The $2p_{3/2}$ core level XPS spectra for $[FeCl_4]^-$ and $KFeS_2$ are shown in Figure 7a, which is adapted from ref 33.

(33) Butcher, K. D.; Gebhard, M. S.; Solomon, E. I. *Inorg. Chem.* **1990**, *29*, 2067−2074.

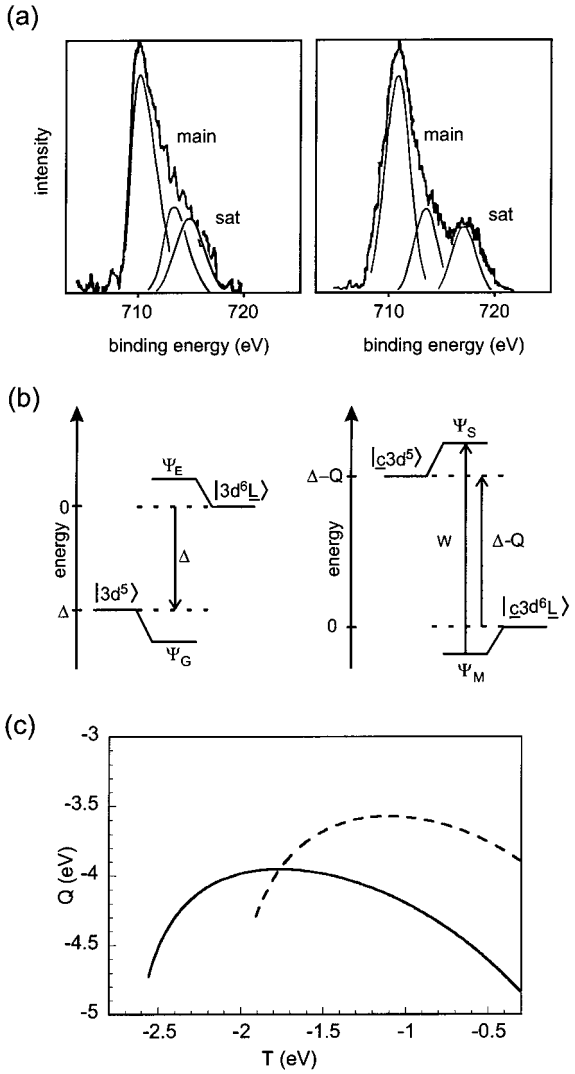

Figure 7. **(a)** Experimental $2p_{3/2}$ XPS spectra of $KFeS_2$ (left) and $Na[FeCl_4]$ (right) adapted from Butcher et al.[33] **(b)** Configuration interaction model for analysis of XPS satellite structure: ground-state configurations (left) and relaxed final state configurations (right). **(c)** Dependence of Q on T for $Na[FeCl_4]$ (—) and $KFeS_2$ (---) calculated from the experimental values for W and I_S/I_M given in Table 4.

In the photoemission process, an electron is ionized from a core level of the ground-state configuration (Ψ_G). Ionization of a metal 2p electron yields the core levels $2p_{3/2}$ and $2p_{1/2}$ which are split through spin−orbit coupling. In the sudden approximation, the creation of the photoelectron hole occurs rapidly, before the remaining electrons adjust to the new potential (configuration Ψ_R). The hole in the core results in final state relaxation because the valence electrons feel a higher effective nuclear charge and

the electron−electron repulsion energies change. For late transition metal ions, the energy level ordering of the valence electron MOs becomes inverted so that in the relaxed final state the antibonding levels have mostly ligand character and the bonding levels are mostly metal-like. This relaxed final state (configuration Ψ_M) corresponds to the main transition in the Fe $2p_{3/2}$ XPS spectrum (Figure 7a). The satellite transition results formally from a two-electron transition corresponding to the simultaneous core ionization plus excitation of an electron from the mainly metal-based orbitals to the mostly ligand-based orbitals (configuration Ψ_S). This formally forbidden two-electron shake-up transition gains intensity from final state relaxation. The intensity (I_i, i = M, S) is given in the sudden approximation as

$$I_i = |\langle \Psi_i^{n-1} | \Psi_R^{n-1} \rangle|^2 \tag{3}$$

where Ψ_i^{n-1} is the respective final state, Ψ_R^{n-1} is the initial unrelaxed state with one electron removed, and n is the number of electrons in the system before ionization. According to eq 3, only initial and final states with the same symmetry can contribute to main peak and satellite formation.

To derive a value for the covalency, a simple valence bond configuration interaction (VBCI) model was applied to the PES data as described by Sawatzky et al.[34] and Davis.[35] The extended model of Park et al.[36,37] was not used because the extension takes into account charge-transfer (CT) transitions corresponding to three or more electronic transitions which are not observed experimentally.

In the VBCI model, the ground-state wave function Ψ_G is obtained from diagonalization of the 2 × 2 matrix

	$\lvert 3d^5 \rangle$	$\lvert 3d^6 \underline{L} \rangle$
$\langle 3d^5 \rvert$	Δ	T
$\langle 3d^6 \underline{L} \rvert$	T	0

(4)

where $|3d^5\rangle$ represents the metal electron valence configuration and $|3d^6\underline{L}\rangle$ represents the one-electron ligand-to-metal charge-transfer configuration before mixing ($\underline{L}$ denotes a ligand hole) (Figure 7b, left). The solution of eq 4 gives

$$\Psi_G = (\cos\theta)|3d^5\rangle - (\sin\theta)|3d^6\underline{L}\rangle \tag{5}$$

for the eigenvector of the lowest energy state with

$$\tan 2\theta = +\frac{2T}{\Delta} \tag{6}$$

By this definition the energy splitting, Δ, is negative (Figure 7b, left). The eigenvalues of the mixed states are

$$E_{\pm} = (1/2)\Delta \pm (1/2)\sqrt{\Delta^2 + 4T^2} \tag{7}$$

The photoemission process creates a core hole denoted by $\underline{c}$. The two possible final states corresponding to the main (Ψ_M) and the satellite (Ψ_S) peaks are

$$\Psi_M = (\cos\theta')|\underline{c}3d^5\rangle - (\sin\theta')|\underline{c}3d^6\underline{L}\rangle \tag{8a}$$

$$\Psi_S = (\sin\theta')|\underline{c}3d^5\rangle + (\cos\theta')|\underline{c}3d^6\underline{L}\rangle \tag{8b}$$

with

$$\tan 2\theta' = +\frac{2T}{\Delta - Q} \tag{9}$$

The energy matrix is then

	$\lvert \underline{c}3d^5 \rangle$	$\lvert \underline{c}3d^6\underline{L} \rangle$
$\langle \underline{c}3d^5 \rvert$	$\Delta - Q$	T
$\langle \underline{c}3d^6\underline{L} \rvert$	T	0

(10)

where Q represents the interaction of the core hole with the electronic state (by this definition $Q < 0$). The energy difference, W, between the main and the satellite peaks is therefore (Figure 7b, right)

$$W = \sqrt{(\Delta - Q)^2 + 4T^2} \tag{11}$$

Combination of eqs 3, 5, and 8 gives the intensity ratio for the main and the satellite transitions as

$$\frac{I_S}{I_M} = \frac{|\langle \Psi_S^{n-1} | \Psi_R^{n-1} \rangle|^2}{|\langle \Psi_M^{n-1} | \Psi_R^{n-1} \rangle|^2} = \left(\frac{\sin\theta'\cos\theta - \cos\theta'\sin\theta}{\cos\theta'\cos\theta + \sin\theta'\sin\theta}\right)^2 = (\tan(\theta' - \theta))^2 \tag{12}$$

With eqs 6, 9, 11, and 12 the system has four equations and seven variables. The energy splitting W and the intensity ratio I_S/I_M of the two XPS transitions are experimentally observed (Figure 7a). The broad features were fit with two Gaussian peaks for the main transition and one Gaussian peak for the satellite region,[33] giving the results for W and I_S/I_M shown in Table 4.

For $[FeCl_4]^-$ the chloride−Fe covalency over all five d-orbitals was determined to be 85.5% by Cl K-edge XAS.[13] Under the assumption of negligible e(π) covalency, the ligand character is 28.5% per t_2 orbital, yielding 71.5% d character. With this input value along with W and I_S/I_M, the remaining four variables could be determined in the four equations listed above (Table 4). Note that the value for $Q = -4.4$ eV is nearly the same as the previously estimated value of $Q = -4.3$ eV for reasonable values of T (Figure 7c).[38]

The value of $\Delta = -2.3$ eV that was obtained for $[FeCl_4]^-$ represents the energy difference between the Fe d-manifold and the Cl 3p manifold before interaction. To obtain a value of Δ for $KFeS_2$, the electronic absorption spectra of both the $[FeCl_4]^-$ and the $KFeS_2$ compounds were analyzed in order to compare

Table 4. XPS Parameters for $[FeCl_4]^-$ and $KFeS_2$[a]

	$[FeCl_4]^-$	$KFeS_2$		$[FeCl_4]^-$	$KFeS_2$
I_S/I_M	0.20	0.31	T (eV)	−2.4	−1.4
W (eV)	5.3	4.2	$\cos^2\theta$, %	71.5	58.0
Q (eV)	−4.4	−3.6	$\cos^2\theta'$, %	30.7	12.3
Δ (eV)	−2.3	−0.4			

[a] Values for I_S/I_M and W for both were obtained from previous studies.[33,38] The value of $\cos^2\theta$ for $[FeCl_4]^-$ was based on previous XAS results.[13]

(34) van der Laan, G.; Westra, C.; Haas, C.; Sawatzky, G. A. *Phys. Rev. B* **1981**, *23*, 4369−4380.
(35) Davis, L. C. *Phys. Rev. B* **1982**, *25*, 2912−2915.
(36) Park, J.; Ryu, S.; Han, M.; Oh, S.-J. *Phys. Rev. B* **1988**, *37*, 10867−10875.
(37) Zaanen, J.; Westra, C.; Sawatzky, G. A. *Phys. Rev. B* **1986**, *33*, 8060−8073.
(38) Butcher, K. D.; Didziulis, S. V.; Briat, B.; Solomon, E. I. *J. Am. Chem. Soc.* **1990**, *112*, 2231−2242.

their ligand-to-metal charge-transfer transitions. The energy difference of the first ligand-to-metal charge-transfer transition ($t_1 \rightarrow e$ in approximate T_d symmetry) gives the shift of the respective ligand 3p manifold. This transition occurs at 3.39 eV in $[FeCl_4]^-$ [39] and at 1.51 eV in $KFeS_2$.[40] The sulfur 3p manifold is therefore 1.88 eV higher in energy in comparison to the chloride 3p manifold. This results in $\Delta = -0.4$ eV for $KFeS_2$. From this the remaining four variables could be determined (Table 4). On the basis of Figure 7c, $Q = -3.6$ eV is the value which one can expect for reasonable values of T. The reduction of Q in sulfide versus chloride ligation of nearly 17% is reasonable due to the larger nephelauxetic effect of the sulfide. On the basis of this analysis, the sulfide covalency per iron orbital in $KFeS_2$ is determined to be 42%, which yields a total covalency of 210%. Note that all Fe d-orbitals are treated approximately as equivalent since the e(π) interaction is now larger for sulfide ligation (vide infra). As $CsFeS_2$ is isostructural with $KFeS_2$, it is assumed in further analysis that their covalency values are the same.

Comparison of the Transition Moment Integral for Thiolate and Sulfide. On the basis of eq 2, and the covalencies obtained for plastocyanin (Pc) and the bis-μ_2-sulfide-bridged compound $CsFeS_2$, the transition moment integral, $\langle 1s|\mathbf{r}|3p\rangle^2$, can be calculated for both thiolate and sulfide, where $\mathbf{r}$ is the electric dipole operator and the integral represents the intensity of a pure $1s \rightarrow 3p$ transition. The value of this integral can be obtained experimentally since the covalency has been determined by XPS and the intensity has been determined from ligand K-edge data. On the basis of the covalency of 38% and an intensity of 1.02 in Pc, the transition moment integral for a thiolate transition is 8.05. (It should be noted as determined in ref 13a that the D_0 expression for Cu(II) is the same as that for Fe(III) except that the integral must be multiplied by 1/3 since there is only one hole in the t_2 set of orbitals while the D_0 expression for Fe(III) is multiplied by 3/3.) The total sulfide covalency of 210% for $KFeS_2$, and by analogy $CsFeS_2$, was determined as discussed above. To determine the transition moment integral on the basis of one Fe−sulfide bond, the total covalency was divided by 4 and the intensity of the pre-edge renormalized to one sulfide, and further divided by 2 to obtain the Fe−S covalency per sulfide per iron. Therefore, the transition moment integral, calculated using 52.5% for covalency and 1.15 for the D_0 value, was determined to be 6.54, which is lower than that of the thiolate by 18%.

Determination of Covalency of the Rieske Cluster. The covalency value reported in Table 3 for the reduced cluster represents the sulfide covalency to the ferric iron site since in the reduced cluster, the sulfide contributions to the ferrous site are obscured by the rising edge. However, the covalency reported for the oxidized protein represents the *average* covalency per sulfide per iron, meaning that a bridging sulfide has a total covalency of 71% times 2, or 142%. Since the S K-edge data of the reduced site represent contributions only from the Fe(III) site (i.e., the ferric site containing terminal thiolate and bridging sulfide ligation), a subtraction of the reduced spectrum from the oxidized spectrum should reveal differences in the covalency of the respective sites, on the basis of the assumption that the electronic structure of the ferric site in the reduced protein does not change significantly upon the oxidation of the adjacent Fe center. This difference spectrum, shown in the inset of Figure 6, was fit independently, but with peaks and criteria similar to those of other fits in this study, and reveals that the sulfide covalency to the iron site of the oxidized Rieske cluster containing terminal histidine ligation is ~80%. Subtraction of this value from the total sulfide covalency in the oxidized Rieske cluster (142%) results in a covalency of 62% to the Fe^{3+} site containing the terminal cysteines. This indicates a small covalency reduction from 67% to 62% by oxidation of the Rieske cluster.

Discussion

Calibration of Iron−Sulfide Covalency. Previously, iron−thiolate covalency has been calibrated from XAS pre-edge studies. In this study, iron−sulfide covalency has been quantified using the PES data of the bis-μ_2-sulfide-bridged infinite chain compound, $KFeS_2$, which is isostructural to $CsFeS_2$.[41] On the basis of previous studies,[42] it was shown that quantification of the valence band region of variable photon energy PES spectra provides information about metal−ligand bonding and covalency. On the basis of the valence band PES spectrum of $[FeCl_4]^-$, and also including the recent XAS study in which the chloride−Fe covalency of this complex was determined, values for T and Δ were obtained (eqs 6, 9, 11, and 12). Using electronic absorption spectroscopy, comparisons were made between the lowest energy charge-transfer transitions of the chloride and sulfide complexes to obtain a value of Δ for the $KFeS_2$. Finally, the value of covalency based on the experimentally derived values for Q, Δ, and T was determined. This is the first study in which sulfur K-edge X-ray absorption spectroscopy has been used for understanding metal−ligand covalency in bridging sulfide bonds.

Having determined the covalency for sulfide, and using the thiolate covalency for Pc, the relative transition moment integrals were experimentally obtained for a pure $1s \rightarrow 3p$ transition for a sulfide and thiolate, respectively. It was found that the intensity for a thiolate transition is larger than that for a sulfide, 8.05 versus 6.54, respectively. The reduction observed in the transition moment integral of ~18% is expected in going from RS^- to S^{2-}. This difference is most likely due to differences in effective nuclear charge on the sulfur centers. Because the valence orbitals are more affected than core orbitals due to changes in effective nuclear charge, the transition moment integral is most affected by the 3p orbitals. In the case of S^{2-} relative to RS^-, there is more electron density, and therefore, the effective nuclear charge for the 3p electrons should be lower in S^{2-}. The expressions of Slater and Clementi[43] show that indeed the effective nuclear charge felt by the 3p electrons of S^{2-} is lower than that of SR^-, leading to less orbital contraction and reduced overlap with the localized 1s orbital in the transition moment integral.

Even though the transition moment integral is lower for the sulfide compared to the thiolate, the calculated covalency is higher. If the thiolate peak of the monomeric $[Et_4N][Fe(S_2\text{-}o\text{-}xyl)_2]$ complex is compared with the sulfide peak of the $CsFeS_2$ complex (Figure 8), it is found that the sulfide peak is more intense. Calculation of the covalencies reveals that for $[Et_4N][Fe(S_2\text{-}o\text{-}xyl)_2]$ the average thiolate covalency for one iron−thiolate bond is ~43%, while in $CsFeS_2$, the average sulfide covalency for one iron−sulfide bond is ~52%. Considering calculations by Noodleman et al.,[44,45] it appears that the increase in sulfide covalency is associated with an increased π interaction

(39) Deaton, J. C.; Gebhard, M. S.; Solomon, E. I. *Inorg. Chem.* **1989**, *28*, 877−889.
(40) Taft, C. A.; De Paoli, M. A. *Chem. Phys. Lett.* **1979**, *68*, 94−96.
(41) Bronger, V. W. *Z. Anorg. Allg. Chem.* **1968**, *359*, 225−233.
(42) Didziulis, S. V.; Cohen, S. L.; Gerwirth, A. A.; Solomon, E. I. *J. Am. Chem. Soc.* **1988**, *110*, 250−268.
(43) Karplus, M.; Porter, R. N. *Atoms and Molecules*; W. A. Benjamin: Menlo Park, CA, 1970.

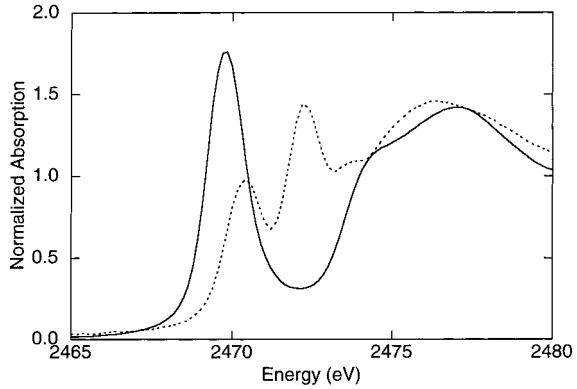

Figure 8. S K-edge spectra of $CsFeS_2$ (—) and $[Et_4N][Fe(S_2\text{-}o\text{-}xyl)_2]$ (···).

in sulfide versus thiolate. This is consistent with the position of S^{2-} within the spectrochemical series. The lower $10Dq$ results from the fact that S^{2-} is a better π donor. This difference in π covalency of sulfide versus thiolate is best considered in the dimeric complexes since the d-orbital splittings are fixed. This will be discussed in the next section.

Comparison of Thiolate and Sulfide Covalency within the 2Fe−2S Models. From Table 3, the thiolate covalency of the fully oxidized 2Fe−2S models decreases per ligand−metal bond relative to the monomeric Fe−S model (∼25−33% versus ∼43%). In contrast, sulfide covalency increases in the $[Fe_2S_2Cl_4]^{2-}$ complex relative to the infinite chain $CsFeS_2$ complex, which has all of its sulfurs bridging between two irons. These two observations lead to the conclusion that the bridging sulfide is more covalent, donating more of its charge to the metal center than terminal thiolate. As suggested in the previous section, the difference in sulfide versus thiolate covalency is most likely due to the greater e(π) donation in the sulfide−metal bond. This can be experimentally evaluated from a comparison of the peak widths of the sulfide pre-edge peak in $[Fe_2S_2Cl_4]^{2-}$ versus the thiolate pre-edge peak in $[Fe_2Se_2(SPh)_4]^{2-}$ (Figure 9). To compare the thiolate pre-edge peak with the sulfide pre-edge peak, theoretical fits of the $[Fe_2S_2Cl_4]^{2-}$ sulfide pre-edge peak and the thiolate pre-edge peak of $[Fe_2Se_2(SPh)_4]^{2-}$ were performed on the basis of calculated d-orbital splitting[44,45] scaled down for final state effects and are shown in Figure 9. In these fits, energy splitting and relative intensities were fixed on the basis of the calculations. These fits gave good results compared to the data. It is observed from these fits that inclusion of the lowest-energy peak with significant intensity, which represents π covalency in one of the orbitals of the T_d e set, in the $[Fe_2S_2Cl_4]^{2-}$ but not in $[Fe_2Se_2(SPh)_4]^{2-}$ pre-edge fit, is necessary to reproduce the experimentally observed difference in the peak widths. Thus, the bridging sulfide ligand has a significant π donor interaction with the iron in contrast to the terminal thiolate ligand.

Comparison of the total covalencies for the monomer with four thiolate sites versus the infinite chain complex with four sulfide sites, 172% thiolate (43% × 4) versus 210% sulfide (52.5% × 4), respectively, shows that the sulfide complex is more covalent (Table 3). When the total sulfide and total thiolate contributions to covalency in the oxidized dimer model containing both bridging sulfide and terminal thiolate, (i.e., $[Et_4N]_2[Fe_2S_2(SPh)_4]$) are summed, the final total sulfur covalency over the d-orbitals is ∼204%, which is more covalent than an iron tetrathiolate monomer, but less covalent than an iron tetrasulfide complex. By comparing the individual contributions to covalency, of which the total sulfide covalency is ∼144% while the terminal thiolate covalency is ∼60%, and the thiolate covalency is less than half the value of the iron tetrathiolate complex, it is concluded that the sulfide contributes more electron donation to the iron site than the thiolate. This is consistent with the trend observed between $[Fe_2S_2Cl_4]^{2-}$ and $CsFeS_2$. Since the $[Fe_2S_2Cl_4]^{2-}$ complex has terminal chlorides instead of all bridging sulfides, the sulfides are expected to be more covalent than the sulfides in $CsFeS_2$. This is because the sulfides are better donors than chlorides, and the smaller charge donation of the chloride to the metal is compensated by the bridging sulfides. Indeed, the sulfide covalency per one sulfide per one iron in $[Fe_2S_2Cl_4]^{2-}$ is ∼65% versus ∼52% sulfide in $CsFeS_2$.

In addition, the energies of the edge and pre-edge features are consistent with this covalency comparison. Since $CsFeS_2$ is less covalent per sulfide−iron bond, the sulfide donates less of its charge to the metal center, resulting in the sulfide core 1s being at lower binding energy. This results in a lower energy edge transition. The energy of the edge feature of $CsFeS_2$ is ∼0.4 eV lower than that of $[Fe_2S_2Cl_4]^{2-}$ (Table 2), whereas the pre-edge feature of $CsFeS_2$ is ∼0.5 eV higher than that of $[Fe_2S_2Cl_4]^{2-}$, which is consistent with the higher total covalency of $CsFeS_2$. The higher covalency results in a lower effective nuclear charge on the metal center, which raises the energy of the d-manifold, and therefore the pre-edge feature is observed at higher energy. Since the edge peak shifted ∼0.4 eV to lower

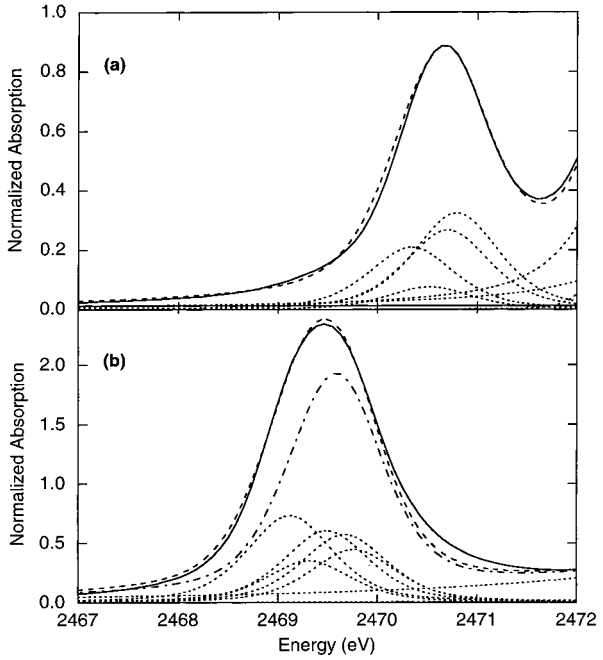

Figure 9. Theoretical fits (---) and experimental spectra (—) of **(a)** $[Et_4N]_2[Fe_2Se_2(SPh)_4]$ and **(b)** $[Et_4N]_2[Fe_2S_2Cl_4]$. From ref 45 the energy splittings of the d-orbitals are 0.24, 0.47, 0.69, and 0.80 eV, which have been scaled by 0.8 for final state effects. Relative intensities of the peaks are fixed on the basis of the calculations. Note that the sulfide contributes to all five transitions whereas thiolate only contributes to four transitions at higher energy.[45] The experimental peak widths (HWHM = 0.55 eV for $[Et_4N]_2[Fe_2Se_2(SPh)_4]$ and HWHM = 0.60 eV for $[Et_4N]_2[Fe_2S_2Cl_4]$) support the differences in the number of peaks required by the calculations. In (b) the sum of the four higher energy peak is also included (-·-), demonstrating the poor quality of the fit without the low-energy peak contribution.

(44) Li, J.; Noodleman, L. In *Spectroscopic Methods in Bioinorganic Chemistry*; Solomon, E. I., Hodgson, K. O., Eds.; American Chemical Society: Washington, DC, 1998; pp 179−195.

(45) (a) Li, J.; Nelson, M. R.; Peng, C. Y.; Bashford, D.; Noodleman, L. *J. Phys. Chem. A* **1998**, *102*, 6311−6324. (b) Li, J., Noodleman, L. Personal communication.

energy, the overall d-manifold shift is ~0.9 eV, corresponding to a covalency increase of 60% per iron.

Chemical Trends Observed within the 2Fe−2S Model System. All the binuclear ferric models in Figure 2 display similar broad pre-edge features. Focusing specifically on the comparison of $[Et_4N]_2[Fe_2S_2(SPh)_4]$ with $[Me_3NCH_2Ph]_2[Fe_2S_2(SEt)_4]$, the edge feature of the latter has shifted to lower energy. This shift is also present in the pre-edge transition. The well-resolved higher energy peak at ~2470.7 eV in $[Et_4N]_2[Fe_2S_2(SPh)_4]$ shifts to lower energy in $[Me_3NCH_2Ph]_2[Fe_2S_2(SEt)_4]$. While this energy shift in the pre-edge feature is consistent with the shift of the edge feature, on the basis of the pK_a values of EtSH versus PhSH, it might be expected that the opposite effect would be observed. The pK_a value for EtSH is 10.61[46] while that for PhSH is 6.43.[47] Typically, increased basicity (higher pK_a) corresponds to increased nucleophilicity (i.e., stronger donor interaction). The opposite experimental trend is likely due to the fact that the pK_a values are determined by the H 1s orbital interaction with one of the orbitals on the sulfur. When the sulfur is bound to the metal center, two 3p orbitals on the sulfur as well as all of the d-orbitals on the metal can participate in metal−ligand π-bonding, and this affects charge donation.

The correlation between the total covalency of the complexes and the reduction potentials can now be investigated. Since both thiolate and sulfide covalencies have been determined in the case of $[Fe_2S_2(SPh)_4]^{2-}$, $[Fe_2S_2(S_2\text{-}o\text{-}xyl)_2]^{2-}$, and $[Fe_2S_2(SEt)_4]^{2-}$, the total ligand covalency is defined. Also, in the case of $[Fe_2S_2Cl_4]^{2-}$ both the S K- and the Cl K-edge spectra have been obtained and their pre-edge features have been quantified. Therefore, the total covalency of $[Fe_2S_2Cl_4]^{2-}$ is also determined. The total ligand covalencies of the $[Fe_2S_2(S_2\text{-}o\text{-}xyl)_2]^{2-}$, $[Fe_2S_2(SEt)_4]^{2-}$, $[Fe_2S_2(SPh)_4]^{2-}$, and $[Fe_2S_2Cl_4]^{2-}$ are 266, 206, 204, and 156%, respectively. Their corresponding reduction potentials are −1.49,[1] −1.31,[1] −1.09,[21] and −0.82[48] mV versus SCE, respectively. It is observed that there is a correlation between total ligand covalency and reduction potential, where a decrease in covalency corresponds to an increase in reduction potential. This is consistent with the idea that increased ligand−metal covalency stabilizes the oxidized site, lowers the effective nuclear charge of the metal, and lowers the reduction potential of the complex.

The effects that changing the terminal and bridging ligands have on covalency are now considered. While the terminal chloride covalency is less than that of the terminal thiolate, the sulfide covalency in $[Fe_2S_2Cl_4]^{2-}$ is similar to that of $[Fe_2S_2(SR)_4]^{2-}$, indicating that the nature of the terminal ligand does not significantly affect the bridging sulfide covalency. In addition, terminal thiolate covalency is not affected by changing the bridging ligation from sulfides to selenides; i.e., the terminal iron−thiolate covalencies for $[Fe_2S_2(SPh)_4]^{2-}$ and $[Fe_2Se_2(SPh)_4]^{2-}$ are similar (Table 3). ^{57}Fe Mössbauer data show that there is no significant difference for the iron in the selenide- versus sulfide-bridged complexes.[49−51] Although the Fe−Se bond is longer than the Fe−S bond, the Se orbitals are more diffuse and closer in energy to the iron d-orbitals, and these two effects compensate. The similarity between the additive spectrum of $[Fe_2S_2Cl_4]^{2-}$ plus $[Fe_2Se_2(SPh)_4]^{2-}$ compared to the spectrum of $[Fe_2S_2(SPh)_4]^{2-}$ (Figure 3b) supports these observations.

Comparison of the 2Fe−2S Models with the 2Fe−2S Rieske Cluster. For the reduced Rieske cluster, the covalency presented in Table 3 represents one Fe(III) center. Comparison of this value of 67% with those of the other fully oxidized dimers shows that the sulfide covalency of the Rieske cluster is lower while the thiolate covalency is comparable with that of the model complexes. There are two effects that could potentially cause this reduction in sulfide covalency within the protein active site. First, since the reduced site contains histidine ligands which are poorer donors, the bridging sulfides could be donating more charge to the iron center. This cannot be evaluated since the pre-edge intensity of a sulfur bound to a ferrous site is at a higher energy and overlaps the rising-edge feature. Also, as noted in our previous study of rubredoxin systems,[15] the experimentally determined H-bonds with the bridging sulfides present in the Rieske cluster[18] but not the models can cause the iron-sulfur covalency to decrease. One might expect that the intensity of the thiolate peak would also decrease in the protein. However, thiolate covalency is very similar between the protein and the models. There are only three hydrogen bonds to the terminal thiolates, and two of these bonds are quite long and would not significantly change the charge on the sulfur.[18] Also, since sulfide covalency decreases, the thiolate covalency could increase somewhat to compensate for the reduced sulfide covalency and therefore counteract the possible effects of H-bonds.

Investigation of the oxidized site of the Rieske protein reinforces the conclusions drawn from the data of the reduced Rieske protein. Again, in this case, independent fits to the data reveal that the thiolate covalency is essentially the same in the oxidized versus the reduced protein as well as the model complexes. On the basis of independent fits, the sulfide covalency in the oxidized protein is asymmetrically distributed over the two ferric iron sites. The Fe^{3+} site containing terminal histidines possesses ~18% more covalency (80% vs 62%) per bridging sulfide. This trend is expected because histidines are poorer donor ligands and the sulfide will donate more charge to this iron center. Additionally, the reduced donor interaction of the histidine ligands is expected to raise the effective nuclear charge on the Rieske center. This is consistent with the high reduction potential of the Rieske cluster, and reinforces the idea that the weak donor interaction of the histidine significantly contributes to this increase in reduction potential.

Ligand K-edge spectroscopy provides a direct experimental probe of covalency in open-shell metal ions. We have used S K-edge spectroscopy to investigate total sulfur covalency in the 2Fe−2S sites of model complexes. Previous studies focused on iron−thiolate bonding, which represents only one type of sulfur present in the 2Fe−2S systems. Therefore, a standard for covalency in an iron−inorganic sulfide bond has been established in this study. Importantly, it is observed that the sulfide can be distinguished from the thiolate pre-edge due to differences in effective nuclear charge. The analysis of both iron−thiolate and iron−sulfide bonding in the model complexes has been developed and then applied to the binuclear site in the Rieske protein. It has been determined that the covalency of the iron−sulfide bond is greater in the iron site of the protein that also contains terminal histidine ligation in contrast to

(46) Danehy, J. P.; Parameswaran, K. N. *J. Chem. Eng. Data* **1968**, *13*, 386-389.
(47) Jencks, W. P.; Salvesen, K. *J. Am. Chem. Soc.* **1971**, *93*, 4433−4436.
(48) Wong, G. B.; Bobrik, M. A.; Holm, R. H. *Inorg. Chem.* **1978**, *17*, 578−584.
(49) Zhou, C.; Holm, R. H. *Inorg. Chem.* **1997**, *36*, 4066−4077.
(50) Yu, S.-B.; Papefthymiou, G. C.; Holm, R. H. *Inorg. Chem.* **1991**, *30*, 3476−3485.
(51) Meyer, J.; Moulis, J. M.; Gaillard, J.; Lutz, M. *Adv. Inorg. Chem.* **1992**, *38*, 73−115.
(52) Mayerle, J. J.; Denmark, S. E.; DePamphilis, B. V.; Ibers, J. A.; Holm, R. H. *J. Am. Chem. Soc.* **1973**, *97*, 1032−1045.
(53) Cai, J.; Cheng, C. *Jiegou Huaxue* **1985**, *4*, 199−202.

terminal thiolate ligation. This illustrates the fact that histidine is a less strong donor than thiolate. This is the first application of S K-edge methodology for the evaluation of covalency in 2Fe−2S iron−sulfur complexes and proteins. This study also provides the basis for quantifying both sulfide and thiolate covalency in the 3Fe−4S and 4Fe−4S systems, which will provide insight into the differences in electronic structure between the 2Fe, 3Fe, and 4Fe sites, attributed to differences in superexchange pathways and electron delocalization.

Acknowledgment. This research was supported by NSF Grant CHE-9528250 (E.I.S.) and Grant CHE-9423181 (K.O.H.) and by NIH Grant RR-01209 (K.O.H.). Stanford Synchrotron Radiation Laboratory operations are funded by the Department of Energy, Office of Basic Energy Sciences. The Biotechnology Program is supported by the National Institutes of Health, National Center for Research Resources, Biomedical Technology Program, and Department of Energy, Office of Biological and Environmental Research. T.G. thanks the Deutsche Forschungsgemeinschaft for a postdoctoral fellowship. We also thank Professor L. Noodleman for providing us with supplementary information concerning the calculations of the 2Fe−2S complexes.

JA983455L